Investigation of wall bounded flows by means of multiple plane stereo PIV

CJ Kähler, M Stanislas+ and T Dewhirst

Deutsches Zentrum für Luft- und Raumfahrt, Institut für Strömungsmechanik
Bunsenstrasse 10, 37073 Göttingen, Germany
email: christian.kaehler@dlr.de
+ Laboratoire de Mécanique de Lille, Bd. Paul Langevin, 59655 Villeneuve D'ASCQ CEDEX, France

ABSTRACT

In order to obtain detailed information about the spatial-temporal flow-unsteadiness in the logarithmic region of a fully developed turbulent boundary-layer flow along a flat-plate, the yz-plane (wall-normal / span-wise) was investigated by means of multiple plane stereo PIV, see Kähler and Kompenhans (1999) for technical details. The experiment was performed in the closed circuit wind tunnel at the Laboratoire de Mécanique de Lille with a 20 m long, 2 m wide and 1 m high test-section, Carlier et al (1999). The thickness of the boundary layer developed at the floor of the test-section was 0.37 m at 3 m/s free-stream velocity and the Reynolds number based on the momentum thickness is 7200. The extent of the logarithmic region measures at least 0.06 m as can be estimated from the upper right plot of figure 1 (average over 1250 independent sample fields each containing 13113 vectors) so that outer-flow effects are negligible over a relatively large domain. The distribution of the velocity fluctuations u′, v′ and w′, the stream-wise vorticity ω_x and two components of the Reynolds stress tensor (v′w′ and u′w′) are exactly symmetrical so that a high flow quality and very accurate alignment of the laser and recording system can be assumed in the following.

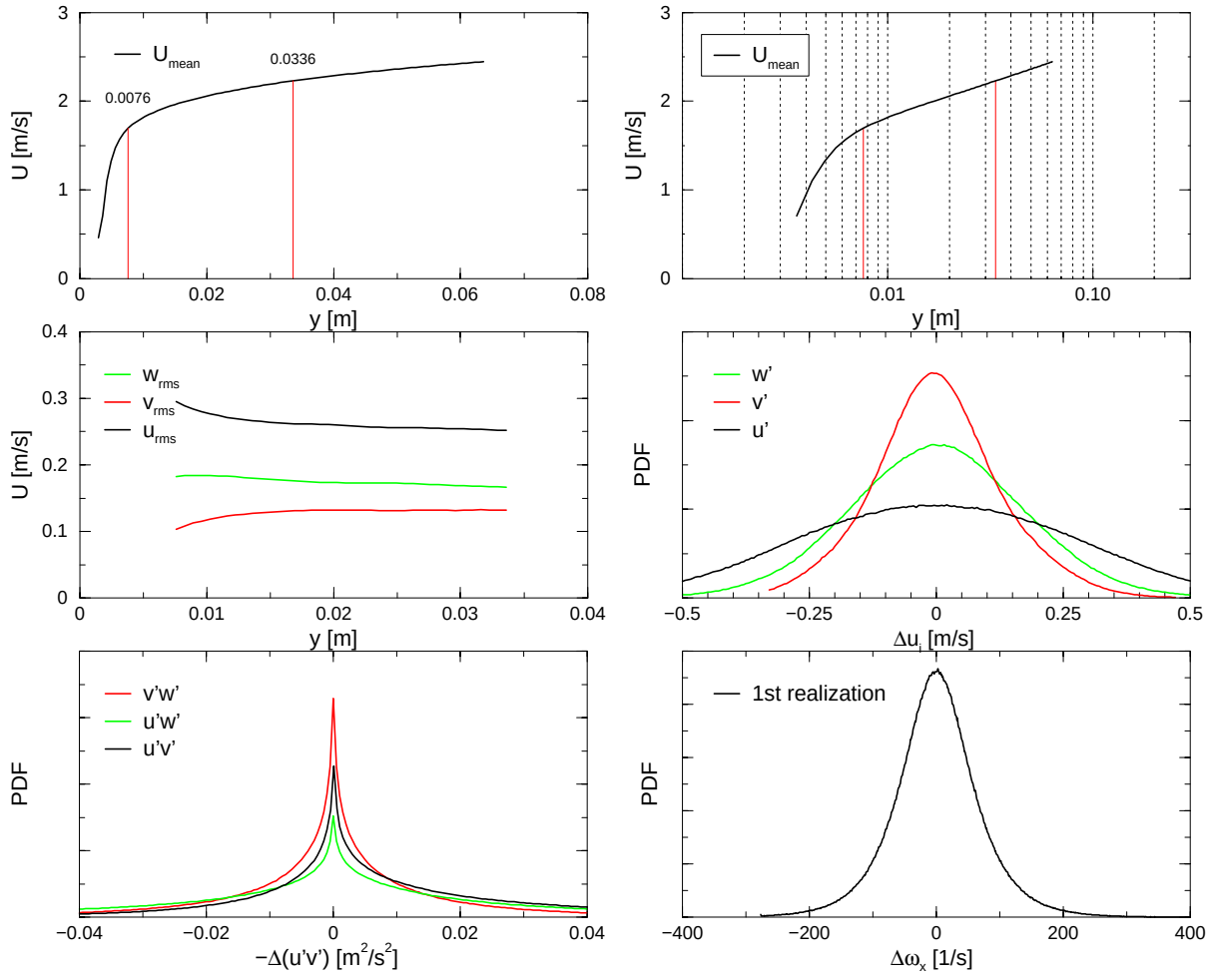

Figure 1. Flow characteristics. Upper row: Mean velocity profile. Center row: Intensities and distribution of the velocity fluctuations. Lower row: Distribution of the Reynolds stresses and stream-wise vorticity.

EXPERIMENTAL CONFIGURATION AND IMAGE ANALYSIS

The multiple plane stereo PIV system in the configuration utilised for this investigation consists of a four pulse Nd:YAG laser-system (BMI) with an output energy of 255 mJ per pulse at λ=532 nm, two independent optical systems for the generation of the light-sheets (one for each polarisation), and four Peltier cooled cameras (PCO) with progressive scan sensor technology, 1280 by 1024 pixel resolution and 12 Bit dynamic range at 12.5 MHz readout frequency. The opening angle between each camera pair in angular imaging configuration with Scheimpflug correction was close to 86° and the observation distance around 2.13 m for all cameras (all asymmetries have been taken into account). Four 180 mm lenses (Carl Zeiss) have been used with an aperture of 8 and a magnification of 1/6 along the principal axis of the lens. For the evaluation of the stereo-scopic images the second order warping technique was applied and additionally a calibration validation method to ensure that the interrogation spots from each of a pair of stereo-scopic images correspond exactly to the same region of flow, see Kähler (2000) for further details. The interrogation of the data was performed with the FFT-based free shape cross-correlation which combines the advantages of the direct correlation (free-sized and free-shaped windows, high accuracy) and the FFT-based correlation (high speed evaluation). For sub-pixel accuracy the two dimensional Gaussian fit using the Levenberg-Marquardt method has been applied to find the position of the correlation peak and the Fisher transformation to determine the weight for each value, Ronneberger et al (1998). For the calculation of the velocity vectors 32×32 pixel^2 interrogation windows were used, corresponding to 1.8 mm^2 in physical space or 12 wall units in each direction. The number of obviously incorrect vectors is on average less than 0.1%, the average height of the correlation coefficient above 0.8 and the range of particle image displacements varies between zero and 8 pixel (zero and –8 for the left camera system in figure 2) for a light pulse delay of 300 µs and 86° opening angle between the observation directions.

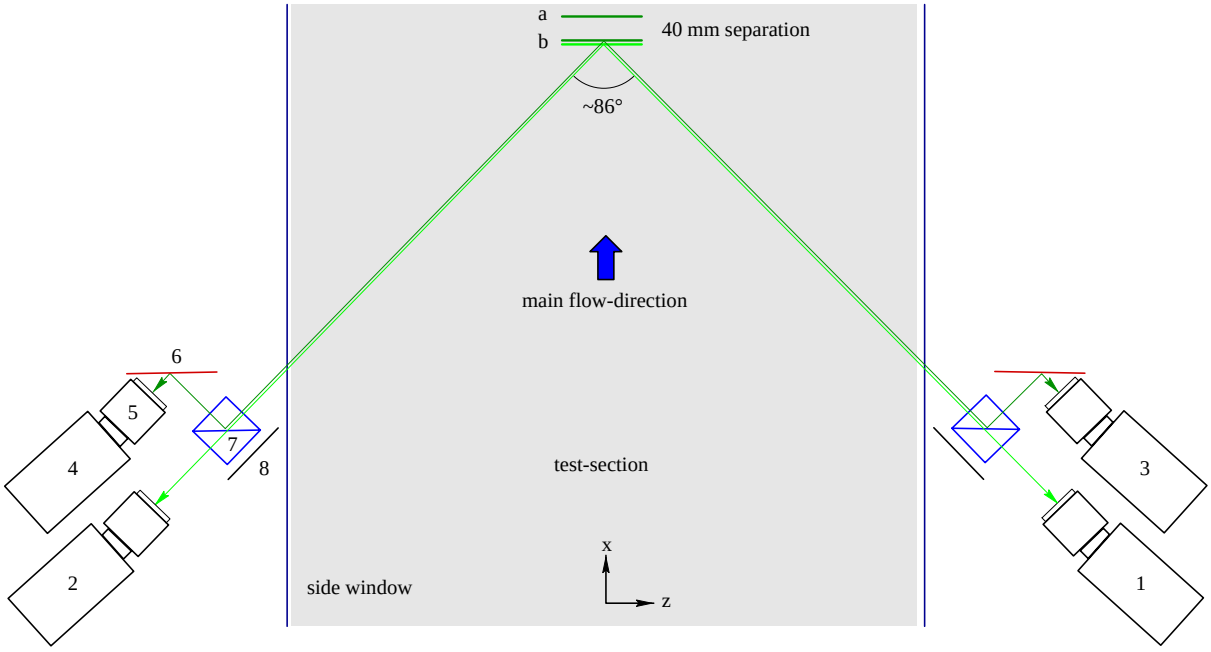

Figure 2. Schematic set-up of the recording system and light-sheet position for both experiments (top view). 1-4 digital cameras, 5 lens, 6 mirror, 7 polarising beam-splitter cube, 8 absorbing material, 9 test-section windows, a measurement location for 1st investigation (40 mm separation between both measurement planes in stream-wise direction), b measurement location for 2nd investigation (all measurement positions at the same location). Different light ray colours indicate different states of polarisation.

In order to avoid that artificial coherent velocity regions, generated by means of a tripping device behind the leading edge of the plate, influence the flow structure, the experiment was performed without disturbing the flow at the beginning of the test-section. Due to the natural transition the exact position of the boundary layer onset remains unknown but this does usually not affect the flow structure near the wall provided the measurement position is sufficiently far behind the transition region and within the range $0 < y/\delta < 0.2$.

SPATIAL-TEMPORAL CORRELATION FUNCTIONS

In this section the average dimensions of the turbulent flow structures will be presented in form of double velocity correlations and their variation with the distance from the wall and the spatial-temporal spacing between the measuring points. The investigation of the spatial correlation tensor of the velocity fluctuations is initiated by the statistical description of turbulence introduced by Reynolds. This approach allows quantitative statements about the average dimensions of the turbulent flow structures and is less complex than considerations based on multidimensional probability distributions, Monin and Yaglom (1973). Several length and time scales with physical meaning can be derived from correlation functions such as the dissipation function or the integral length scale which plays a dominant role in the transport equations proposed by Rotta (1972). In the following the u-component (perpendicular to the light sheet) indicates the main flow direction and the two in-plane components v and w the wall-normal and span-wise components. The axes in stream-wise, wall-normal and span-wise direction are denoted by x, y and z as shown in figure 2. Two similar experiments have been performed independently. In one experiment the spatial location of all light-sheet planes was identical and the time separation between a pair of velocity fields being acquired was altered in order to study the changes of the velocity structures with time, see figure 4 and 5. In another experiment, which will be described first, the time-separation between a pair of measured velocity fields was altered as well but in addition the measurement planes have been spatially shifted in stream-wise direction by 40 mm ($\Delta x^+ \approx 300$) as indicated in figure 2. Thus it was possible to select a flow-structure pattern at an upstream position and to measure the structural changes as a function of spatial distance between the light-sheet pairs and the time interval between the acquisition of the data. As the flow structures and their spatial organisation changes while they are transported downstream, the various correlation values yield information about their life history.

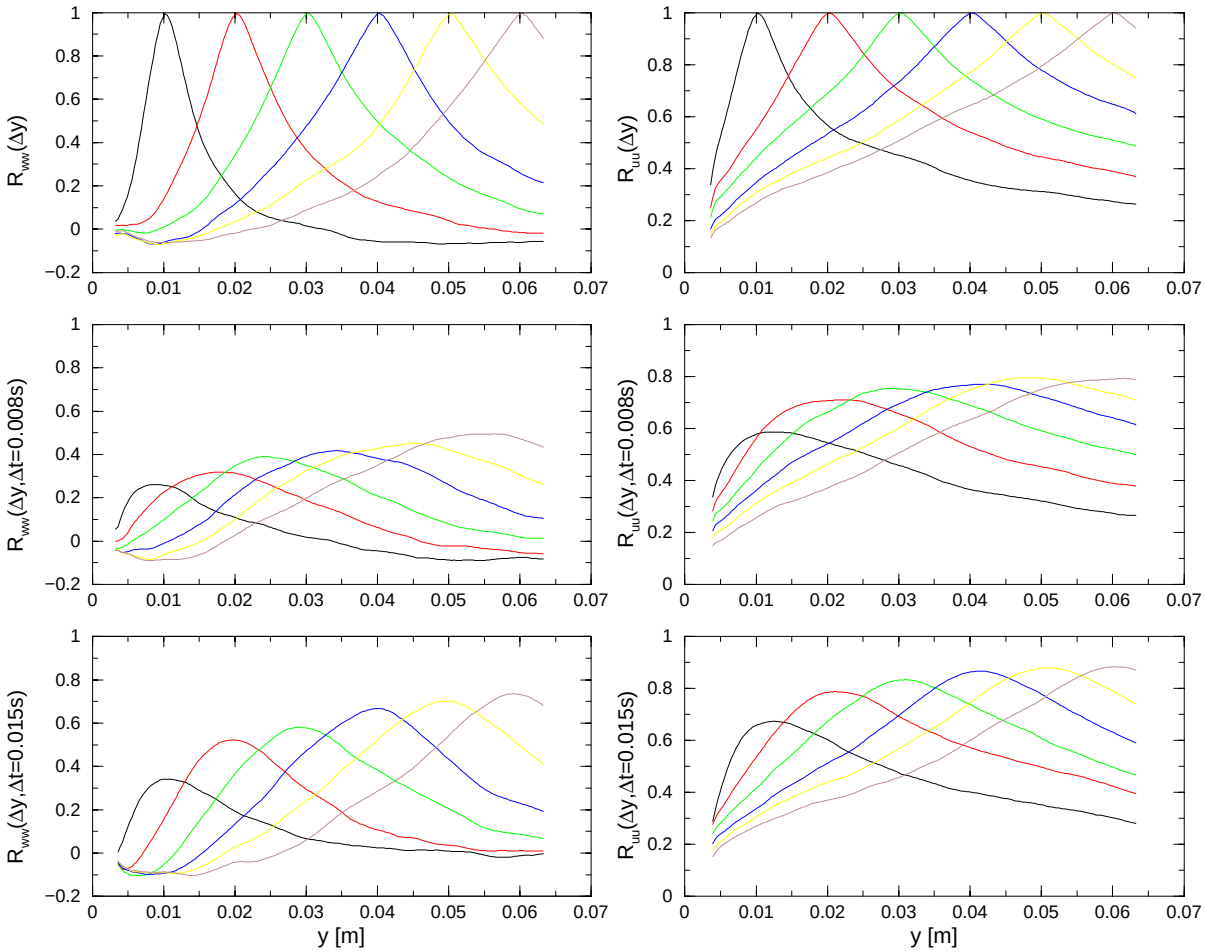

Figure 3. Primary correlation for various wall distances as a function of the y-coordinate and time separations Δt. The spatial separation between the fixed points for the correlation is 10 mm as can be seen from the y location of the maximum value. 10 mm equals approximately 75 wall units and 60 mm corresponds roughly to 0.15 y/δ.

The first row of figure 3 shows for $\Delta t=0$ the primary correlation's $R_{ww}(y)$ and $R_{uu}(y)$ for various distances from the wall (y=10, 20, 30, 40, 50, 60 mm). Clearly visible is the variation of the width and shape of the correlation as a function of wall distance (black line close to the wall, red line further away and so on), the different coherence length between $R_{ww}(y)$ and $R_{uu}(y)$ and the negative correlation range for R_{ww} due to continuity. The second row of figure 3 shows the same correlation functions but estimated by cross-correlating the measurements acquired at different locations (40mm separation between both measurement planes) whereby the downstream measurement was performed 0.008s after the up-stream measurement. As the local mean velocity is approximately 2 m/s according to figure 1, the structures selected at the up-stream location are convected by 16 mm on average or 40% of the distance between the measurement planes. The maximum correlation value is thus relatively low especially near the wall due to the short correlation length (compare graphs in the upper right plot of figure 3) and low local convection velocity. For $\Delta t=0.015$s (lower row of figure 3) the travelling distance is around 30mm or 75% of the separated measurement planes. All correlation maxima increase gradually (up to 0.9 for R_{uu} and large y) whereby the maximum correlation remains again lower for the near wall cases ($R_{uu}<0.7$). As the difference in height is quite large, structural changes or variation in the organisation of the structures closer to the wall (strong variation of the structure location from one time-step to the next) must be the cause for this effect.

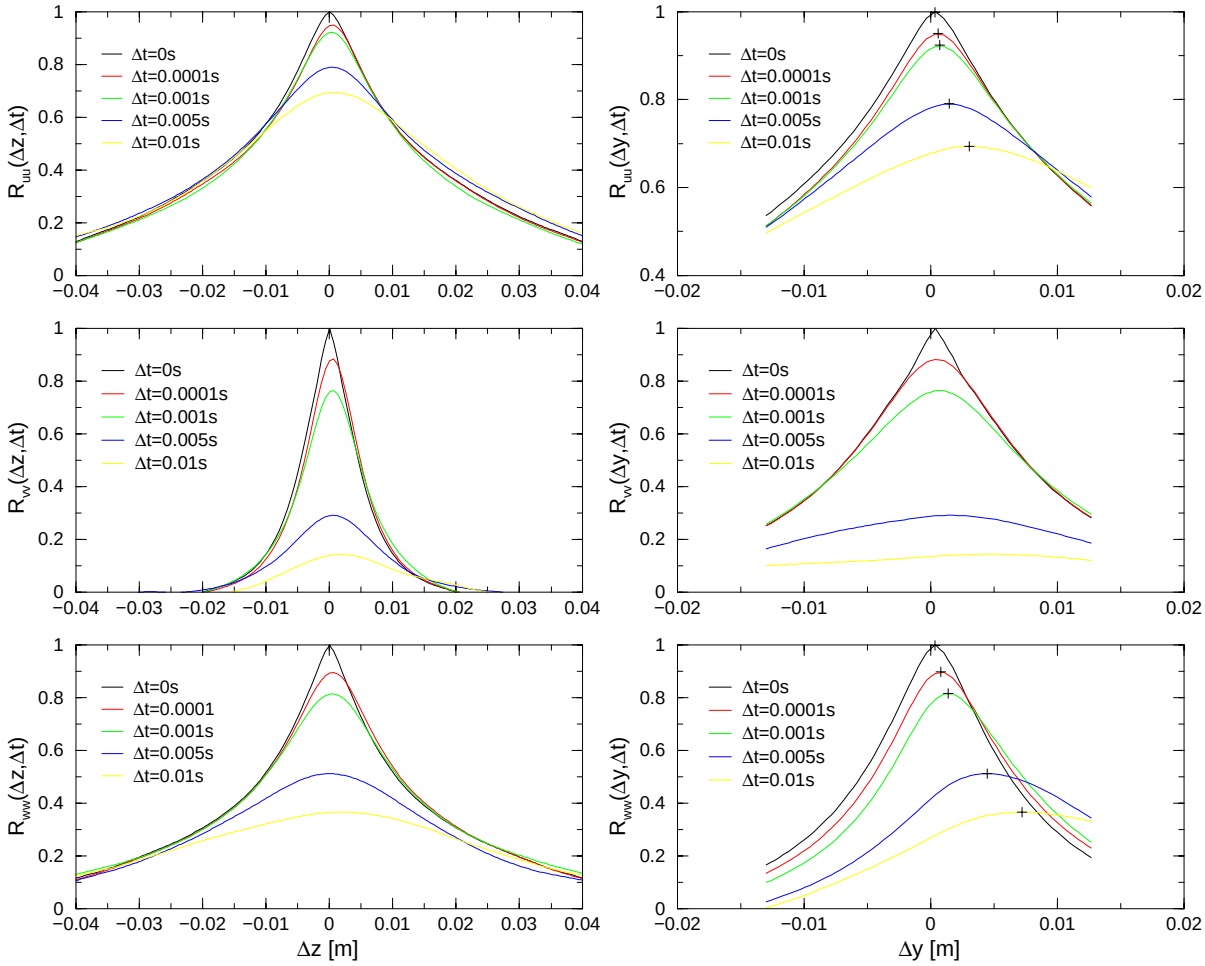

Figure 4. Primary spatial temporal correlation functions for one distance from the wall (20 mm) as a function of the span-wise and wall normal coordinate for different time separations (note variations in the axis scale). The crosses in the top and bottom plot on the right hand side indicate the maximum of the correlation function in order to highlight the correlated upward motion of the fluid with increasing Δt. 10 mm equals approximately 75 wall units and 60 mm corresponds roughly to 0.15 y/δ.

Figure 4 shows all primary correlations as a function of the span-wise coordinate z (left column) and the spatial direction perpendicular to the wall (right column) for different Δt measured at $y\approx20$ mm. The distance between both measurement planes is zero in order to study the convective decay of the flow structures. In order to obtain these graphs a two-dimensional correlation was performed from which two orthogonal lines parallel to the

coordinate axis have been extracted whereby the location of the global maximum was used to select the location of the lines to be extracted (the correlation function depends on the coordinates of the points of which the values have been taken). It should be noted that the $R_{vv}(z)$ correlation is very narrow with respect to the other primary correlations so that the extent of regions where Reynolds stresses are produced must be quite local as well (see also top and middle row of figure 5). Another important fact is the shift of the $R_{uu}(y)$ and $R_{ww}(y)$ towards larger wall distances with increasing Δt. This indicates a highly ordered fluid motion away from the wall, some hundred wall units in length, or alternative a shear layer in stream-wise direction (other interpretations are also possible). As the point of maximum correlation is known along with the time separation, the angle could be roughly approximated by 20° taking the local mean velocity into account. The decreasing correlation value for increasing Δt on the other hand can be interpreted as a measure for the length of the dominant flow structures (at least further away from the wall where Taylor's hypothesis holds).

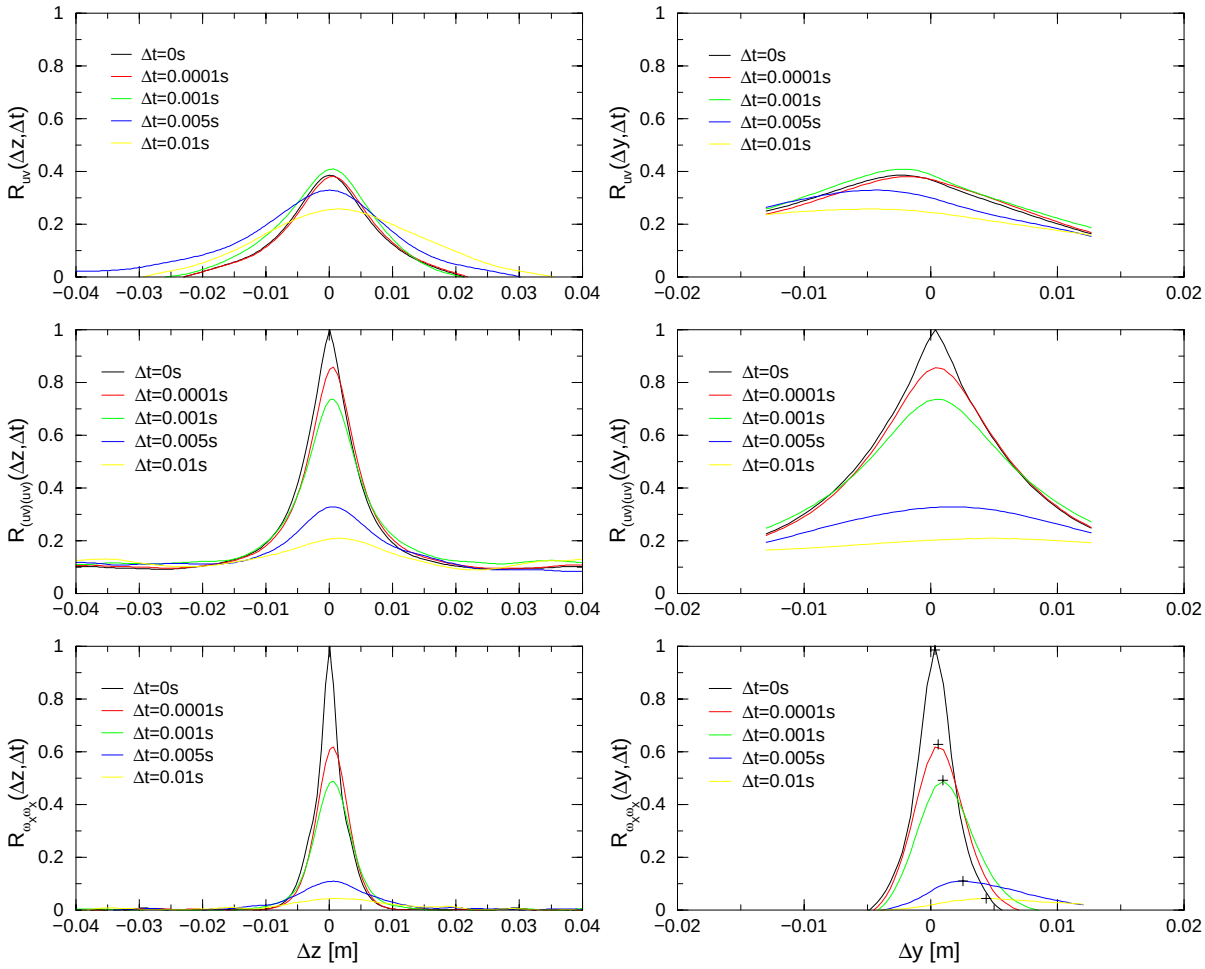

Figure 5. Top row: Correlations of stream-wise and wall-normal fluctuations as a function of the time-separation and spatial coordinate. Center row: Correlation function of the main Reynolds stress component. Bottom row: Correlation function of the stream-wise vorticity component as a function of space and time.

In order to estimate the relation between the stream-wise and wall-normal fluctuations and the average dimension of the flow structures responsible for the production of the Reynolds stresses, $R_{uv}(y,z)$ as well as $R_{(uv)(uv)}(y,z)$ have been calculated (top and center row of figure 5). First of all it should be noted that the maximum of $R_{uv}(y, z)$ increases slightly with increasing Δt before the correlation goes down to zero for $\Delta t \rightarrow \infty$. This indicates that possibly some phase relation exists between the velocity fluctuations in stream-wise and wall-normal direction.Clearly visible is also the rapid decay of $R_{(uv)(uv)}$ for increasing Δt which is mainly due to the small correlation length of R_{vv} (compare with figure 4). The bottom row of the same figure shows the correlation of the stream-wise vorticity as a function of the time separation and spatial direction. The correlated motion of the vortical structures away from the wall is again clearly visible but the spatial-temporal correlation length is extremely small with respect to all other correlation functions. This can be interpreted either by the length of the stream-wise vortices (approximately 20 mm) or their strongly twisted nature for examplel. A decision between

both models can not be made from the correlation measurements as these details are smeared out by the statistical approach. Therefore the instantaneous velocity fields need to be analyzed in detail.

CONCLUSIONS

The aim of this investigation was to demonstrate the power of the multiple plane stereo PIV technique for complex flow analysis. Therefore the spatial temporal behaviour of the flow structures within the span-wise / wall-normal plane of a fully developed turbulent boundary layer was determined in form of spatial / temporal correlation functions of the velocity fluctuations, the Reynolds stresses and the stream-wise vorticity component. Although the stream-wise and span-wise fluid-motion is not remarkably correlated (not shown in this paper) the behaviour of their spatial-temporal correlation functions is quite similar (shape, size and temporal decay). Also the characteristic shift of the largest correlation value towards higher velocity regions with time agrees well. The wall-normal correlations on the other hand are relatively small and their maximum decreases fast with increasing time. This limits the spatial extent of regions where Reynolds stresses are produced. The correlation function of the stream-wise vorticity component shows as well a short spatial-temporal correlation length and in addition a displacement towards higher velocity regions.

REFERENCES

Carlier J, Foucaut JM, Dupont P, Stanislas M (1999) Caractérisation d'une couche limite turbulente à grand nombre de Reynolds par anémométrie à fils chauds et par Vélocimétrie par Images de Particules, 35ème colloque d'Aérodynamique Appliquée, Analyse et contrôle des écoulements turbulents, Lille France

Kähler CJ, Kompenhans J (1999) Multiple plane stereo PIV – Technical realization and fluidmechanical significance, 3rd International Workshop on PIV, University of California-Santa Barbara, USA, paper PIV96, Sept. 16-18

Kähler CJ (2000) Multiplane stereo PIV – Recording and evaluation methods, EUROMECH 411, Rouen, France, May 29-31

Monin AS, Yaglom AM (1973) Statistical fluid mechanics, MIT Press

Ronneberger O, Raffel M, Kompenhans J (1998) Advanced evaluation algorithms for standard and dual plane particle image velocimetry, 9th Int. Symp. on Appl. of Laser Techn. to Fluid Mechanic Lisbon Portugal, paper 10.1, June 13-16

Rotta C (1972) Turbulente Strömungen, B.G. Teubner Stuttgart.